**(Preprint) AAS 18-262**

# SEARCHING FOR ORBITS AROUND EQUILIBRIUM POINTS IN A BINARY ASTEROID SYSTEM MODELED AS A MASS DIPOLE

**Santos, L. B. T.,[1] Sousa-Silva, P. A.,[2] Sanchez, D. M.,[3] Prado, A. F. B. A [4]**

The objective of the present work is to search for orbits around the equilibrium points $L_1$ and $L_2$ of the restricted three-body synchronous problem (RTBSP). From the equations of motion of a binary system of asteroids, where one of the asteroids is modeled as a rotating mass dipole, it was possible to determine the initial conditions for Lyapunov orbits. The study was carried out by modifying the mass ratio of the system and the size of the dipole mass in rotation. By linearizing the equations of motion, it is possible to obtain the eigenvectors and eigenvalues, and with these values, it was possible to determine the initial estimates to find periodic orbits around the equilibrium points using Newton's method. Then a family of orbits was built around the equilibrium points $L_1$ and $L_2$.

## INTRODUCTION

The interest in analyzing, investigating and understanding the dynamics of a satellite around the equilibrium points has grown in recent years, due to the advantages that these points offer when it comes to space missions[1]. Several space missions near the collinear equilibrium points have been completed, are in execution or are being prepared for the near future[2-4]. The ISEE-3 was released in 1978 and inserted a spacecraft into a periodic orbit in the vicinity of the equilibrium point $L_1$ of the Sun-Earth system with the objective of making studies of the Earth-Sun interactions[5, 6]. This was the first artificial object to be sent to an equilibrium point. Its main mission was to investigate the structure of the solar wind in the vicinity of the Earth, among others[1, 3]. Since then, several space agencies have considered periodic or quasi-periodic orbits around the libration points as target-orbits for their spacecraft, as used with the satellites SOHO[7], MAP, ACE, Genesis, among others, and there are several future projects that intend to use orbits around equilibrium points to develop their missions, such as NGST, Herschel-Planck, James Webb Space Telescope, that will succeed of Hubble Space Telescope and that has the intention of orbiting the equilibrium point $L_2$ of the Sun-Earth system[1, 8, 9]. From the twentieth century, several researches have contributed to a better understanding of the CRTBP, but the action of several disturbing forces were not taken into account in many of these problems. The classical model does not consider some of the disturbing forces, such as the irregular shape of one of the primary bodies, the Poynting-Robertson drag effects, the solar radiation pressure, and the mass ratio variations of the primaries. Some of the expressive works in the CRTBP were produced by references[10-15].

[1] PhD Student, Division of Space Mechanics and Control, National Institute for Space Research - INPE, Astronautas Avenue 1758, São José dos Campos-SP, Brazil, 12227-010.

[2] Professor, Department of Mathematics, São Paulo State University - UNESP, São João da Boa Vista – SP

[3] Post-doctoral Fellow, Division of Space Mechanics and Control, National Institute for Space Research - INPE, 12227-010 São José dos Campos, Brazil

[4] President of the Board of the Graduate School at INPE in Brazil, National Institute for Space Research - INPE, 12227-010 São José dos Campos, Brazil

To perform this study, we used a model based on rotating dipole mass, first introduced by Chermnykh (1987)[16]. Kokoriev and Kirpichnikov (1998)[17, 18] were also one of the pioneers to use this model. It is considered in this model that the gravitational field of two bodies of point masses located on the axis of symmetry of an asteroid closely approximates the gravitational field of an axially symmetrical body. In this work, one of the bodies of the asteroid binary system is modeled as a rotating mass dipole, representing in this way as an elongate body.

This model used in asteroid was developed by Zeng et al. (2015)[19]. In the work of Ferrari et al. (2016)[20], a way of finding trajectories in the vicinity of a binary system, using the dipole model in one of the asteroids (Zeng et al., 2016e)[21], was analyzed. Ferrari (2016)[20] also analyzed these trajectories and studied the effects of the flyby using an analytical approach and finding an important relation between the flyby and the integral of Jacobi. Santos, Prado and Sanchez (2017)[22] analyzed the restricted problem of three bodies using the rotating mass dipole model, in which was investigated the behavior of the equilibrium points when the mass ratio of the system and the dipole dimension are modified. An interesting relation was found between the linear stability of the equilibrium points as a function of the dipole dimension. Santos, Prado and Sanchez (2017)[23] also analyzed the behavior of the collinear equilibrium points when the two primary bodies are considered as a mass dipole in synchronous rotation. Santos, Prado and Sanchez (2017)[24] investigated the lifetime of a spacecraft that orbits an asteroid binary system in which one of these bodies is modeled as a rotating mass dipole. Numerical evidence has shown that retrograde orbits around this type of system survive longer than direct orbits.

In this work, we intend to find planar Lyapunov orbits around the equilibrium points $L_1$ and $L_2$ around a binary asteroid system, where the more massive asteroid is modeled as a mass point, and the other one is modeled as a rotating mass dipole. After finding the Lyapunov orbits, we intend to obtain families of orbits around these equilibrium points. Analyzes will be performed using analytical and numerical methods. For the analytical study, the linearization of the equations of motion will be performed, and from there, the necessary initial guess will be obtained, to find the Lyapunov orbits around the libration point. Once the initial guesses are found, it will be possible, through iterative numerical methods, to find a solution of the non-linearized problem.

## EQUATION OF MOTION

In this study, we developed the equation of motion of a body with infinitesimal mass, when attracted by the gravitational forces of two massive bodies ($M_1$ e $M_2$), where the smallest primary is modeled as a rotating mass dipole. In this analysis, we consider that the rotational period of the less massive body ($M_2$) around its axis is equal to its period of translation around the center of mass of the system, making the movement to be synchronous. The unit of distance was chosen to be the distance from the center of mass of the body $M_1$ to the center of mass of the body $M_2$, where the latter is formed by two hypothetical bodies with masses $m_{21}$ and $m_{22}$, according to Figure 1.

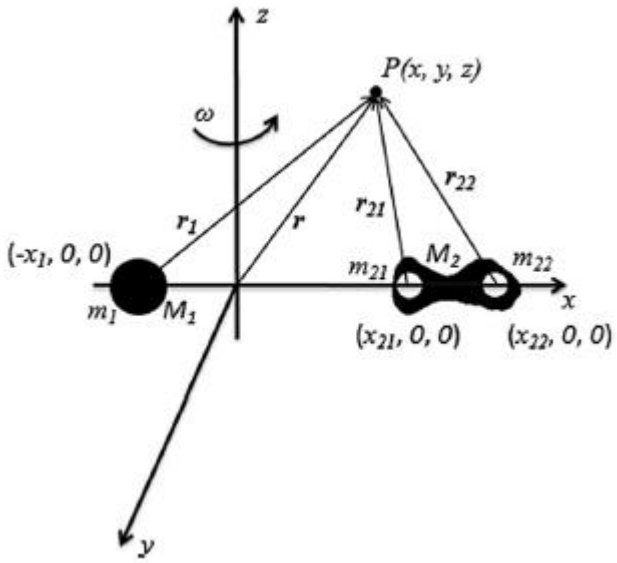


**Figure 1. Image of the geometric shape of the system analyzed. Figure taken from[22].**

By taking convenient units of mass, time and length (canonical units), it is possible to simplify the equations of motion. Every equation is developed in the *x*-*y* plane, when viewed from a synodical reference system, where the origin is defined as the mass center of the system. In this rotating system, the primary with larger mass ($M_1$) has mass $m_1 = 1\text{-}2\mu^*$ and it is always located at $x_1 = (-2\mu^*, 0)$. The masses of the two hypothetical bodies that form the body $M_2$ are $m_{21} = m_{22} = \mu^*$, and they are located in the $x_{21} = (-2\mu^* + 1 - d/2, 0)$ and $x_{22} = (-2\mu^* + 1 + d/2, 0)$, respectively, where $d$ is the distance between the bodies $m_{21}$ and $m_{22}$. After making some mathematical simplifications, using the canonical units mentioned above, it is possible to find the Hamiltonian function, which is given by:

$$H = \frac{(p_x + y)^2 + \left(p_y + x\right)^2}{2} - \frac{x^2 + y^2}{2} - \frac{1 - 2\mu^*}{r_1} - \frac{\mu^*}{r_{21}} - \frac{\mu^*}{r_{22}}, \tag{1}$$

where

$$r_1 = \sqrt{(x + x_1)^2 + y^2}, \tag{2}$$

$$r_{21} = \sqrt{(x + x_{21})^2 + y^2}, \tag{3}$$

$$r_{22} = \sqrt{(x + x_{22})^2 + y^2}, \tag{4}$$

and $p_x$ is the angular momentum of the particle relative to the axis $x$ and $p_y$ is the angular momentum of the particle relative to the axis $y$. From the Hamiltonian function, it is possible to determine the equations of motion of an infinitesimal mass particle when viewed from a rotating reference system, which is given by

$$\dot{x} = \frac{\partial H}{\partial p_x} = p_x + y, \tag{5}$$

$$\dot{y} = \frac{\partial H}{\partial p_y} = p_y - x. \tag{6}$$

The remaining dynamical equations are

$$\dot{p}_x = \frac{-\partial H}{\partial x} = p_y - x + \Omega_x, \tag{7}$$

$$\dot{p}_y = \frac{-\partial H}{\partial y} = -p_x - y + \Omega_y, \tag{8}$$

where $\Omega_x$, $\Omega_y$ are the partial derivatives of $\Omega$ with respect to *x* and *y*, respectively[25], where

$$\Omega = \frac{x^2+y^2}{2} + \frac{1-2\mu^*}{r_1} + \frac{\mu^*}{r_{21}} + \frac{\mu^*}{r_{22}}. \tag{9}$$

From the Lagrangian formulation it is possible to write the equations of motion. To do this, it is necessary to make the transformation $\dot{x} = p_x + y$, $\dot{y} = p_y - x$, where $\dot{x}$ and $\dot{y}$ are the velocities of the particle as seen from a rotating reference system. In this way, the equations of motion can be written as follows:

$$\ddot{x} - 2\dot{y} = \Omega_x \tag{10}$$

$$\ddot{y} + 2\dot{x} = \Omega_y \tag{11}$$

Equations (10) and (11) have the same appearance of the equation of motion of the restricted classical three-body problem, that has been extensively studied in the scientific community[26, 27].

The is also a constant in this problem, which is the Jacobian integral[24]. It is given by

$$v^2 = 2\Omega - C^*, \tag{12}$$

where $C^*$ is a modified integral constant, analyzed in reference[22].
It is noteworthy that Equation (12) is a function which is dependent on $\Omega$ and an integration constant $C^*$, which is an integral of the equations of motion[28, 29]. In this study, it is assumed that the body with negligible mass is moving in the *x*-*y* plane. Then Eq. (12) shows that, for a given value of $C^*$, the velocity is a function that depends on the position of the body in the plane of motion. The integration constant $C^*$ is dependent on the initial position and velocity of the particle[27]. We can see that Eq. (12) relates the square of the velocity to the coordinates of the body with negligible mass in the rotating coordinate system[29]. Therefore, when determining the integration constant $C^*$ numerically from the initial conditions, by Eq. (12) it is possible to determine the velocity of the particle with negligible mass at all points in space. Conversely, for a given velocity, from Eq. (12) it is possible to determine the geometric shape at the locations where the movement of the spacecraft is allowed. In particular, if we define velocity as zero in Eq. (12), it is possible to find a region where the velocity of the particle is zero[30]. In mathematical terms, these zero velocity curves are defined by $2\,\Omega - C^* = 0$[25]. Writing this in Cartesian coordinates, we obtain Eq. (13):

$$\frac{x^2+y^2}{2} + \frac{1-2\mu^*}{r_1} + \frac{\mu^*}{r_{21}} + \frac{\mu^*}{r_{22}} = C^* \tag{13}$$

The motion of the spacecraft is only possible in regions where $2\,\Omega > C$, otherwise, the square of the velocity needs to be negative, which is impossible from a physical analyses[22].
Although similar, the equations of motion developed in this work differs from the ones of the Restricted Classic Three-Body Problem by the pseudo-potential used in the Equations (10-11). The equilibrium solutions with respect to the rotating system occur when the partial derivative of the pseudo-potential function is equal to zero, that is, $\Omega_x = \Omega_y = 0$, and $\dot{x}$ and $\dot{y} = 0$. These solutions are known as equilibrium points corresponding to fixed positions in the rotating system, where there is a balance between the gravitational and the centrifugal forces that is

associated with the rotation of the system. These equilibrium solutions makes a particle positioned at one of these points to appear stationary in the rotating system[31].
The differential correction method, based on Newton's method, is a powerful tool, which uses the State Transition Matrix (STM) to solve several boundary value problems. The equations of motion studied here have anti-symmetric terms due to the Coriolis acceleration coming from the rotating system. These terms would first to remove any symmetry in the problem. Although not trivial, it is possible to note that the RTBSP has symmetry. The geometry of the configuration space is undoubtedly symmetrical with respect to the rotating system on the *x*-axis. Furthermore, the collinear equilibrium points are on the *x*-axis and the equilateral equilibrium points are symmetrical with respect to the *x*-axis. We can note that the potential function for the system studied here depends only on the distances that a spacecraft are from the primary bodies, that is, it has symmetry with respect to the *x*-axis. Taking advantage of the fact that the planar Lyapunov orbits are symmetrical with respect to the *x*-axis, the initial state vector takes the form

$$\boldsymbol{X}_0 = [x_0, 0, 0, v_{y_0}]^{\mathrm{T}}.$$

These symmetries were used to find symmetric periodic orbits. This is done by determining the initial conditions, on the *x*-axis, where the initial velocity is perpendicular to this axis ($v_y$), and then the integration is done until the path returns by crossing the *x*-axis with the speed orientation $v_{y_f}$ opposite to the initial condition. This orbit can be used as an initial guess to use Newton's method, where the target state is quoted above; that is, that the orbit returns to *x*-axis with normal velocity. The equations of motion and the State Transition Matrix are incorporated numerically until the trajectory crosses the *x*-axis again. The final desired condition has the following form

$$\boldsymbol{X}_f = [x_f, 0, 0, v_{y_f}]^{\mathrm{T}}.$$

**RESULTS**

The initial conditions obtained for the system under study, using the mass ratio of $\mu^* = 0.005284$ for the classical case, $d = 0$, using the differential correction are:

i) For the Lyapunov orbit around $L_1$, when the dipole dimension is zero, is

$$X_{0L1} = \begin{bmatrix} 0.89696483 \\ 0 \\ 0 \\ -0.3370635541809143 \end{bmatrix}$$

with a time period of 3.083 canonical unit.

ii) For the Lyapunov orbit around $L_2$, when the dipole dimension is zero, is

$$X_{0L2} = \begin{bmatrix} 1.18638324 \\ 0 \\ 0 \\ -0.2609113622544423 \end{bmatrix}$$

with a time period of 3.54 canonical unit.

The Lyapunov orbits around $L_1$ and $L_2$ are shown in Figures 2 and 3, in red and green, respectively.

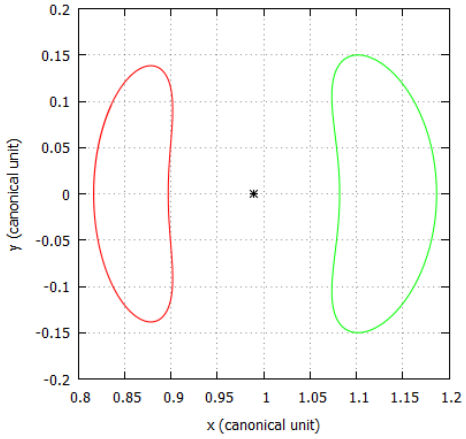


**Figure 2. Lyapunov orbit around $L_1$ (red) and $L_2$ (green). The body $M_2$ plotted in black.**

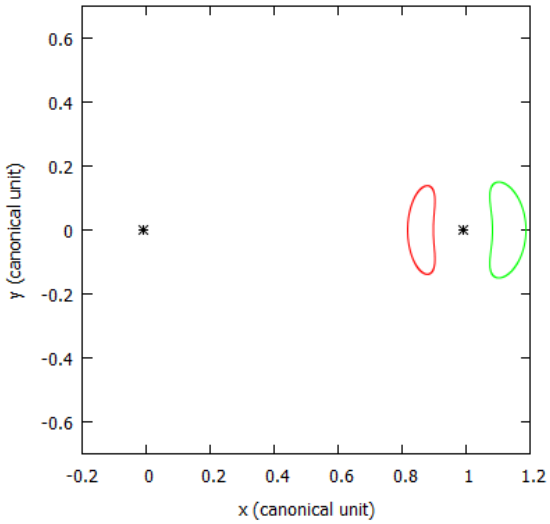


**Figure 3. The primary bodies plotted with black dots and the Lyapunov orbit around $L_1$ (red) and $L_2$ (green).**

## Lyapunov orbits with the addition of the dimensions of dipole.

Some numerical results were obtained for a non zero dimension of the dipole and $\mu^* = 0.005284$. Several values of dimension $d$ of $M_2$ were assumed, modifying the dimension of the rotating mass dipole from 0 to 500 meters, every 100 meters. The purpose of this variation is to understand how the dimension of the dipole influences the Lyapunov orbits near $M_2$, that is, around the equilibrium points $L_1$ and $L_2$.

The results shown here were obtained for $C^* = 3.10$, for which the necks around $L_1$ and $L_2$ are opened. With the correct initial conditions, it was possible to find Lyapunov orbits around the equilibrium points $L_1$ (red) and $L_2$ (green), as shown in Figure 4.

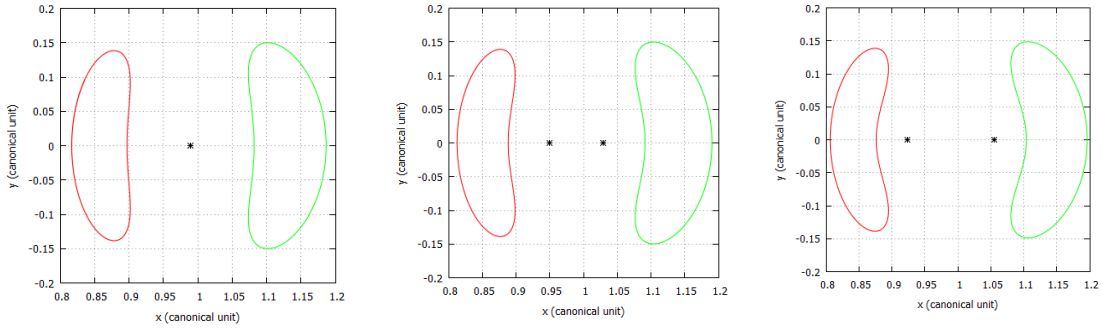


**Figure 4: Lyapunov orbits around equilibrium points $L_1$ (red) and $L_2$ (green).**

Figure 3 shows that, as we increase the dipole dimension, the Lyapunov orbits become more deformed, with a kidney-like shape. Note that the dipole dimension practically does not change the amplitude of the Lyapunov orbit. In the left Figure the dipole dimension is zero, that is, the body $M_2$ becomes a mass point. In the middle figure the dipole dimension is 300 meters, and, finally, in the figure on the right side, the dipole dimension is 500 meters.

Figure 5 a) shows the Lyapunov orbits around points $L_1$ and $L_2$. The caption on the upper right side relates the dimension of the dipole (in meters) with the color of the orbit. When Lyapunov's orbit is green, for example, this implies that the dimension of the dipole is 500 meters. Figure 5 b) is a zoom of the Lyapunov orbit around $L_1$ which is closest to the dipole. We can verify through Figure 5 b) that, as we increase the dimension of the dipole, the orbit becomes more deformed.

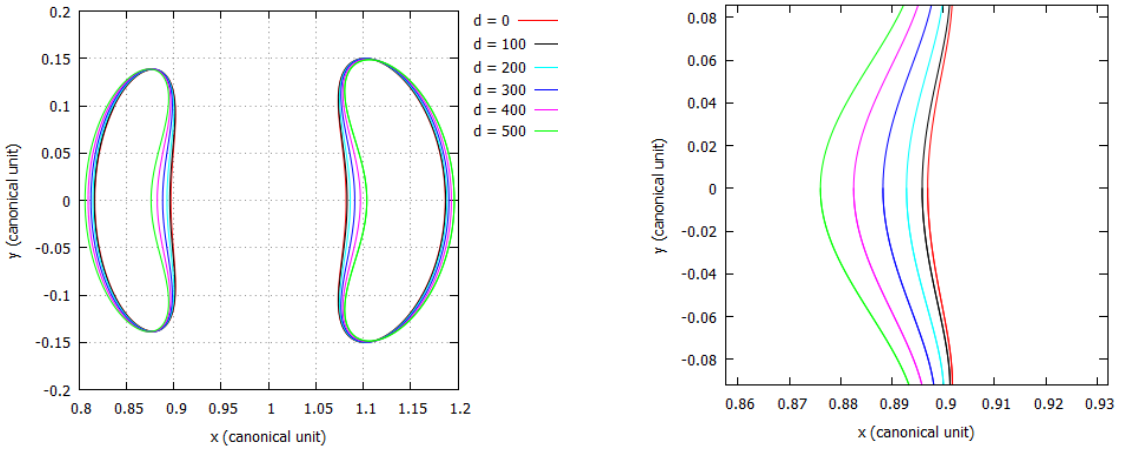


a) Lyapunov orbit considering the Jacobi constant of $C^* = 3.10$.

b) Zoom around the Lyapunov orbit around $L_1$ (of Figure a) which is closest to the dipole.

**Figure 5. Lyapunov orbit around the equilibrium points L1 and L2 for various dipole dimensions.**

Although the dimension of the dipole does not affect the amplitude of the orbit considerably, it influences the period of the orbit. As the dipole size increases, for $C^* = 3.10$, the orbital period of the Lyapunov orbit around the equilibrium point $L_1$ and $L_2$ decreases, as shown in Figure 6 a) and b), respectively.

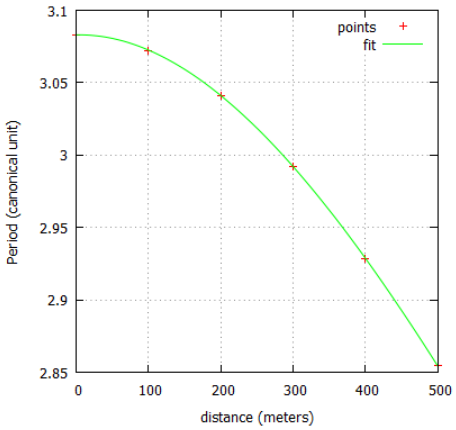


a) Period of the Lyapunov orbit as a function of the dipole dimension for the equilibrium point $L_1$ using the Jacobi constant $C^* = 3.10$.

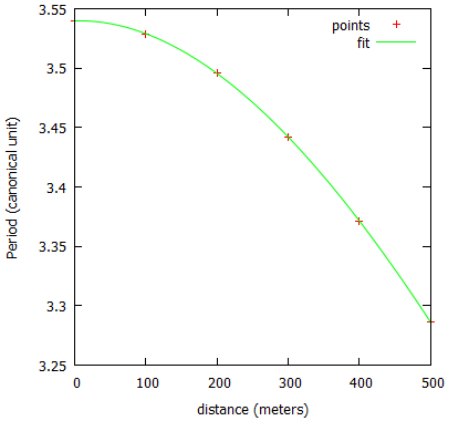


b) Period of the Lyapunov orbit as a function of the dipole dimension for the equilibrium point $L_2$ using the Jacobi constant $C^* = 3.10$.

**Figure 6. Period of the Lyapunov orbit as a function of the dimension of the dipole.**

We note that the amplitude of the Lyapunov orbit around $L_1$ is smaller with respect to the amplitude around $L_2$, which makes its period to be smaller, due to the fact that the spacecraft describes a smaller trajectory.

The curve fit was made in order to find an analytical expression relating the period of the Lyapunov orbits to the dipole dimension, for $C^* = 3.10$. The analytical expression found from the curve fitting for the orbital period as a function of the dipole dimension around the equilibrium points $L_1$ and $L_2$ was a third degree polynomial, as shown in Equations (14) and (15), respectively

$$T_{L_1^{3,10}} = 5.52 \times 10^{-10} d^3 - 1.21 \times 10^{-6} d^2 + 1.21 \times 10^{-5} d + 3.08 \quad (14)$$

$$T_{L_2^{3,10}} = 4.54 \times 10^{-10} d^3 - 1.27 \times 10^{-6} d^2 + 1.53 \times 10^{-5} d + 3.54 \quad (15)$$

in which the upper and lower subscript of the period T indicates the Jacobi constant used for this expression and the related equilibrium point, respectively.

Figures 7 and 8 show the Zero Velocity Curves (ZVC), a Lyapunov orbit (blue) around the equilibrium points $L_1$ and $L_2$, respectively, the most massive primary modeled as a mass point (red asterisk), the less massive primary modeled as a mass dipole rotation (black asterisk) and the positions of the equilibrium points (circles). The Jacobi constants corresponding to these figures is $C^* = 3.10$, for which the necks around $L_1$ and $L_2$ are open. The dipole dimension of 500 meters and a mass ratio of $\mu^* = 0.005284$ were used to obtain these figures,

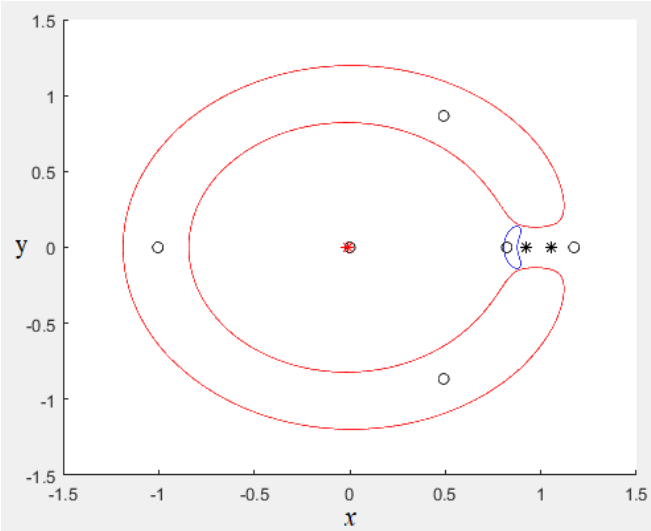


**Figure 7. Lyapunov orbit around $L_1$ equilibrium point and zero velocity curve. Jacobi constant $C^* = 3.10$.**

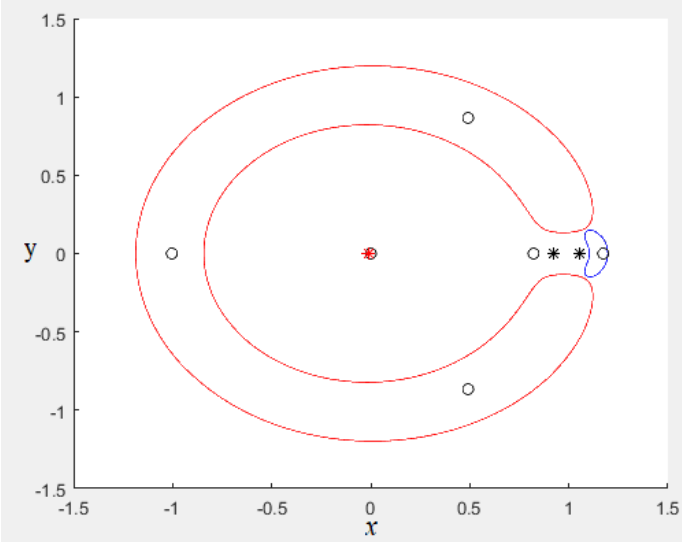


**Figure 8. Lyapunov orbit around $L_2$ equilibrium point and zero velocity curve. Jacobi constant $C^* = 3.10$.**

From the Lyapunov orbits found, using a continuation strategy, it was possible to find families of orbits around the equilibrium points under study. These families of Lyapunov orbits are shown in Figures 9 and 10. The software used was based on the one developed by J.D. Mireles James, with some modifications made to suit the system under study [32, 33]. A family of orbits was constructed around the equilibrium points $L_1$ and $L_2$, as shown in Figures 8 and 9, respectively.

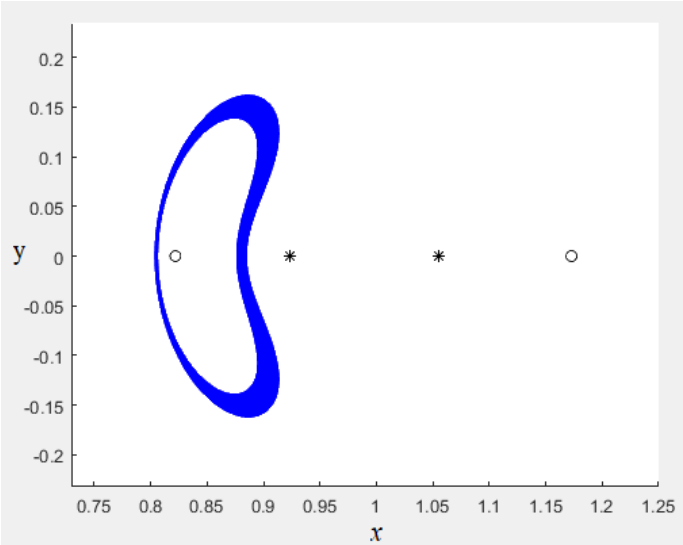


**Figure 9. Family of Lyapunov orbits around $L_1$ equilibrium point.**

It can be seen, from Figures 9 and 10, that, as we increase the amplitude of the Lyapunov orbits, they approach the less massive primary body, making the orbits to become more and more deformed, assuming a kidney shape. If the elongated form of the less massive primary was not taken into account, these orbits would be less deformed, and the infinitesimal mass particle would follow another trajectory.

The black asterisks, near the equilibrium points $L_1$ and $L_2$, are the bodies of masses $m_{21}$ and $m_{22}$, respectively, that form the mass dipole. The circles are the positions of the equilibrium points $L_1$ (left side) and $L_2$ (right side).

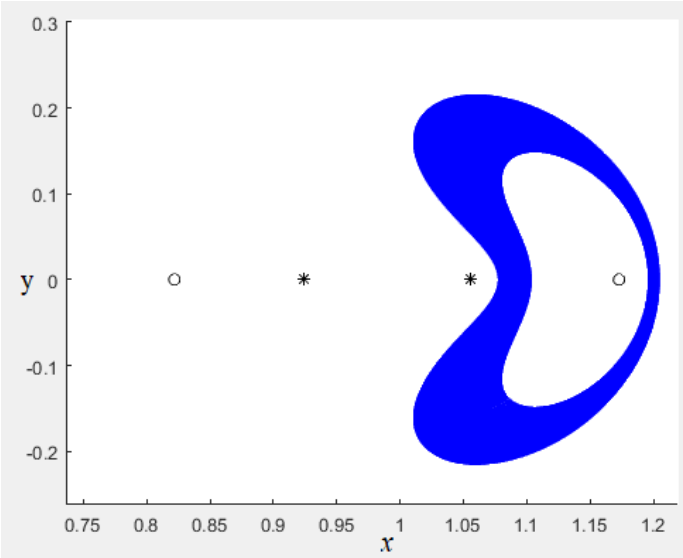


**Figure 10. Family of Lyapunov orbits around equilibrium point $L_2$**

By decreasing the Jacobi's constant to $C^* = 3.01$, the forbidden regions decrease, thereby increasing the regions where the motion of the spacecraft is allowed. The results shown here

were obtained using $C^*$ = 3.01, which allows the neck at $L_1$ and $L_2$ to be opened. With the correct initial conditions, it was possible to find Lyapunov orbits around the equilibrium points $L_1$ and $L_2$, as shown in Figure 11.

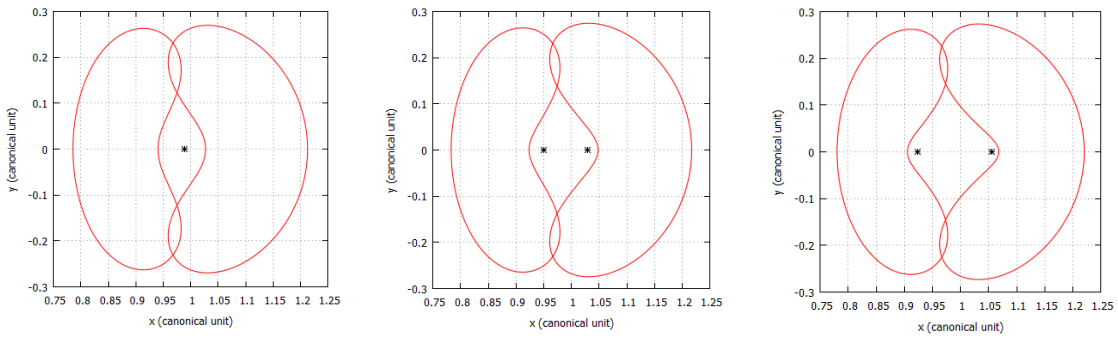


**Figure 11. Lyapunov orbits around equilibrium points $L_1$ (left) and $L_2$ (right).**

We note that, when the Jacobi's constant decreases, there is an increase in energy, causing the orbit's amplitude to increase with respect to the previous figures.

We can see, from Figure 12, that, as we increase the dipole dimension, the Lyapunov orbits become more deformed. Note that the dipole dimension practically does not change the amplitude of the Lyapunov orbit. In the left plot the dipole dimension is zero, that is, the body $M_2$ becomes a mass point. In the middle plot the dipole dimension is 300 meters and, finally, in the plot on the right side the dipole dimension is 500 meters.

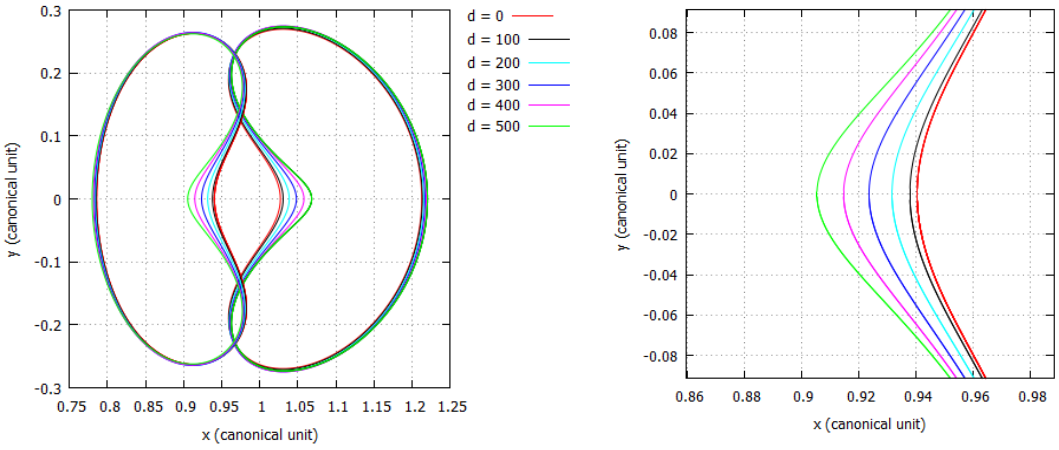


a) Lyapunov Orbit considering $C^*$ = 3.01.

b) Zoom of the closest to the dipole Lyapunov orbit around $L_1$ (Figure a).

**Figure 12. Lyapunov orbit around equilibrium points $L_1$ (left) and $L_2$ (right).**

Figure 12 a) shows the Lyapunov orbits around points $L_1$ and $L_2$ with the Jacobi constant $C^*$ = 3.01. The caption on the upper right side relates the dimension of the dipole (in meters) with the color of the orbit. When the Lyapunov orbit is pink, for example, this implies that the dimension of the dipole is 400 meters. Figure b) is a zoom around the Lyapunov orbit around $L_1$. We verify that, as we increase the dimension of the dipole, the orbit becomes more deformed.

In order to understand how the amplitude of these orbits behaves as a function of the dipole size, the upper region of the orbits around the equilibrium point $L_2$ was zoomed and shown in Figure 13.

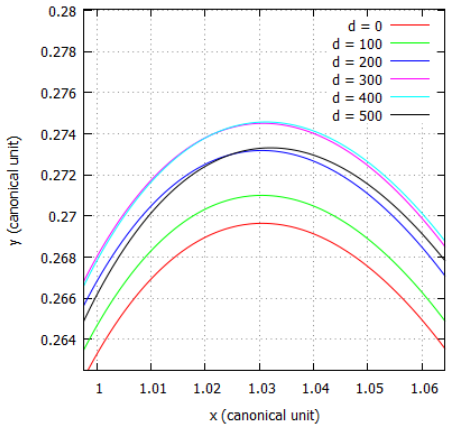


**Figure 13. Amplitude of the Lyapunov orbits considering the Jacobi constant $C^* = 3.01$**

We can see that the amplitude of the orbit differs very little as we change the dipole dimension. The amplitude of the variation of the system under study is 0.004967 canonical units, which is equivalent to 18.89 meters.
Notice that, for this case, the period of the orbit becomes larger as we increase the dipole dimension. This is due to the fact that, when the energy of the spacecraft increases, the orbit becomes increasingly deformed as we increase the dipole dimension. As the orbit becomes more deformed, the path traveled by the spacecraft becomes larger, increasing its the orbital period. Although when the spacecraft is near the dipole the acceleration is larger, because the gravitational field is more intense, the deviation that the spacecraft suffers is considerable, making the time to complete a period to be relevant. This can be observed by looking at the Figures 14 a) and 14 b).

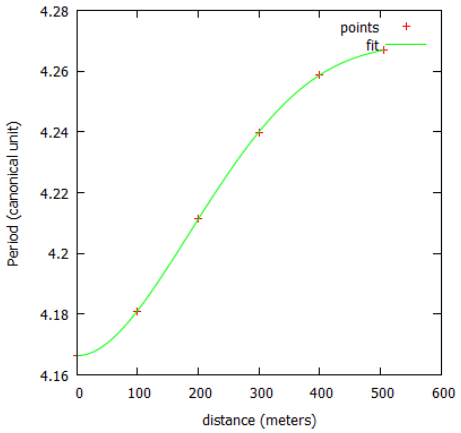


a) Period of the Lyapunov orbit as a function of the dipole dimension for the equilibrium point $L_1$ using the Jacobi constant $C^* = 3.01$.

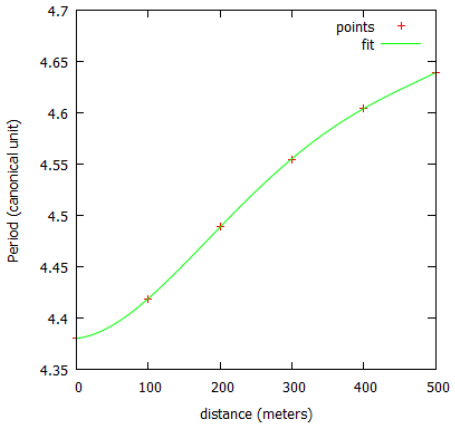


b) Period of the Lyapunov orbit as a function of the dipole dimension for the equilibrium point $L_2$ using the Jacobi constant $C^* = 3.01$.

**Figure 14. Period of the Lyapunov orbits as a function of the dimension of the dipole.**

The period of the orbit around $L_2$ is larger because its amplitude is larger with respect to the Lyapunov orbit around $L_1$. The curve fit was made in order to find an analytical expression relating the period of the Lyapunov orbits to the dipole dimension, for $C^* = 3.01$. The analytical expression found from the curve fitting for the orbital period as a function of the dipole

dimension around the equilibrium points $L_1$ and $L_2$ was a fourth degree polynomial, as shown in Equations (16) and (17), respectively

$$T_{L_1^{3,01}} = 3.33 \times 10^{-12} d^4 - 4.78 \times 10^{-9} d^3 + 1.96 \times 10^{-6} d^2 - 4.45 \times 10^{-6} d + 4.16 \quad (16)$$

$$T_{L_2^{3,01}} = 7.92 \times 10^{-12} d^4 - 1.04 \times 10^{-8} d^3 + 4.13 \times 10^{-6} d^2 + 6.93 \times 10^{-5} d + 4.38 \quad (17)$$

in which the upper and lower subscript of the period T indicates the Jacobi constant used for this expression and the related equilibrium point, respectively.

Figures 14 and 15 show the Zero Velocity Curves (ZVC) when the dipole dimension is 500 meters and the mass ratio of the system is $\mu^* = 0.005284$. Figure 14 and 15 show the Lyapunov orbit (blue) around the equilibrium points $L_1$ and $L_2$, respectively, the most massive primary (red asterisk), the less massive primary (black asterisk) and the positions of the equilibrium points (circles). The Jacobi constant related to these figures is $C^* = 3.01$, where it is possible to allow the neck at $L_1$ and $L_2$ to be opened.

Due to the decrease of the Jacobi constant with respect to the previous cases (Figures 6 and 7), the energy of the system is increased, making forbidden areas where the movement is prohibited to become smaller, as we can see in Figures 15 and 16.

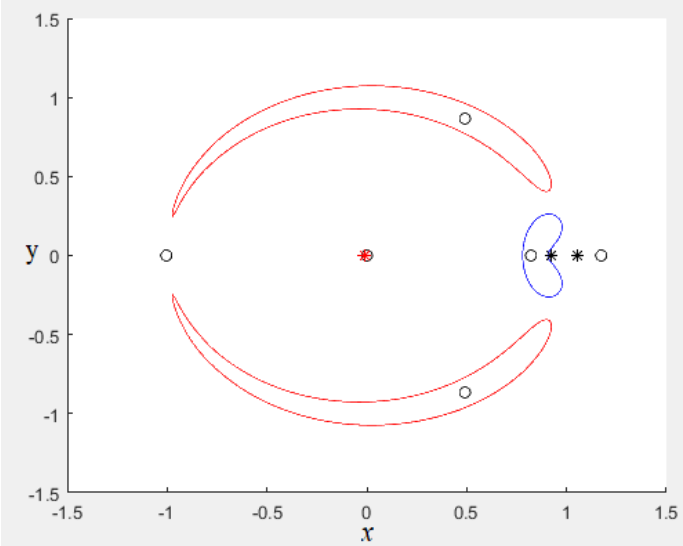


**Figure 15. Lyapunov orbits around $L_1$ equilibrium points and zero velocity curves. Jacobi constant $C^* = 3.01$**

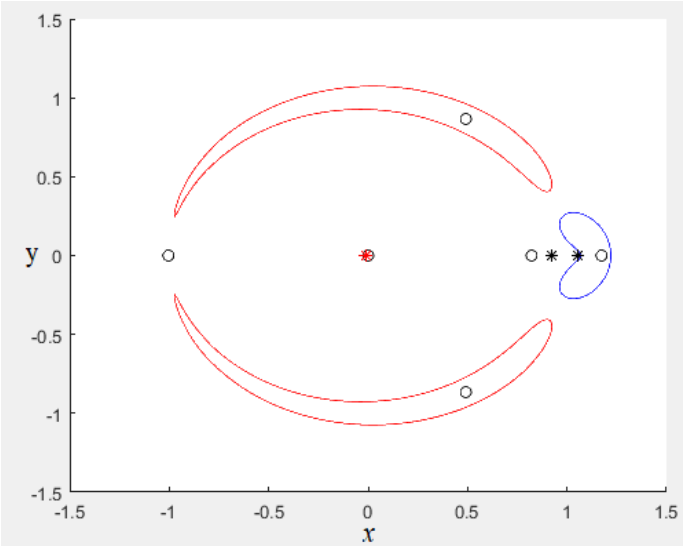


**Figure 16. Lyapunov orbits around $L_2$ equilibrium points and zero velocity curves. Jacobi constant $C^* = 3.01$**

From the Lyapunov orbits found, using a continuation strategy, it was possible to find families of orbits around the equilibrium points. These families of Lyapunov orbits are shown in Figures 17 and 18. A family of orbits was constructed around the equilibrium points $L_1$ and $L_2$, as shown in Figures 17 and 18, respectively.

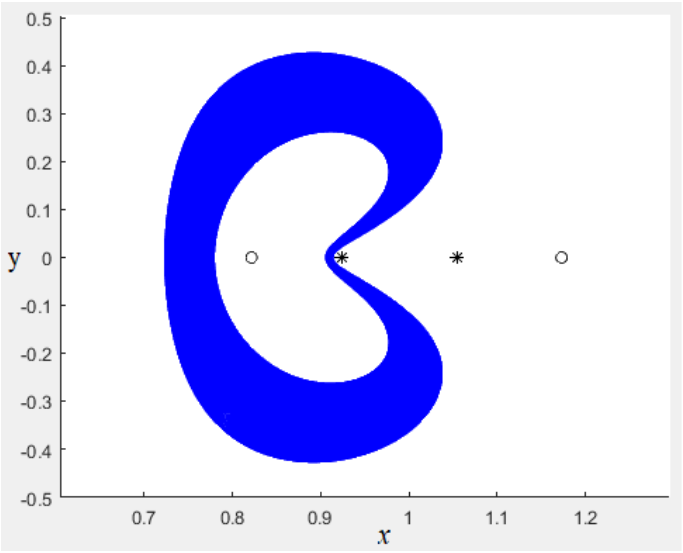


**Figure 17. Family of Lyapunov orbits around equilibrium point $L_1$.**

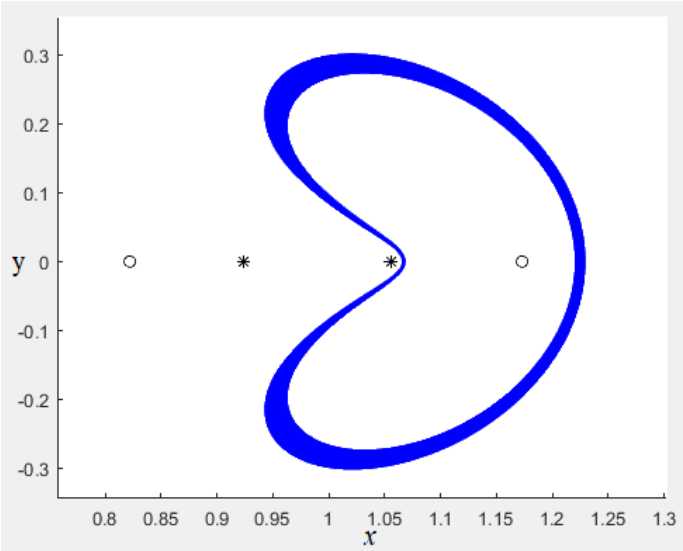


**Figure 18. Family of Lyapunov orbits around equilibrium point $L_2$.**

This analysis was performed for $C^* = 3.01$ because there is the possibility of finding natural orbits that connect the families of orbits around $L_1$ with families of orbits around $L_2$. Due to the symmetry of the Lyapunov orbits with respect to the $y$ axis, we intend to search for homoclinic and heteroclinic orbits in this region of the space under study in future works.

## Lyapunov Orbits with increased mass ratio.

In this section, the work consists in investigating the Lyapunov orbits when we keep the rotating mass dipole constant and modify the mass ratio of the system. The dimension of the dipole is kept constant in the value $d = 250$ meters. This study is performed by modifying the mass ratio of the system. We considered situations where the mass of the less massive primary (dipole) has the values of 0.05, 0.1, 0.15 and 0.2. These values make $M_1$ to become less massive and, consequently, $M_2$ becomes more massive. Figure 19 shows the Lyapunov orbits for various mass ratios, considering the Jacobi constant $C^* = 3.10$.

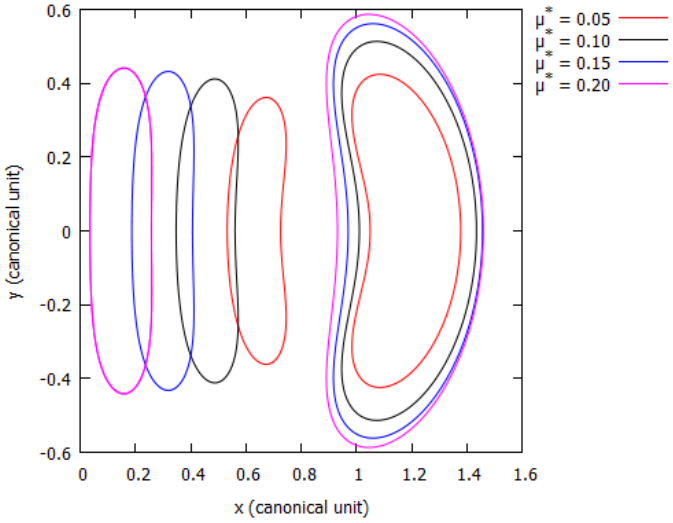


**Figure 19. Lyapunov orbits around the equilibrium points $L_1$ and $L_2$ for different mass ratios. $C^* = 3.10$.**

The color of the orbits is related to the mass ratio of the system. When the mass ratio is $\mu^*$= 0.1, for example, the curve is black. It can be seen from Figure 19 that, as we increase the mass ratio of the system, the equilibrium point $L_1$ shifts considerably, causing the orbits around this bridge to shift as well, following the movement of the equilibrium point $L_1$. On the other hand, the equilibrium point $L_2$ moves very little, which makes the orbits around this point to become concentric. Due to the fact that, as we increase the mass ratio of the system, the equilibrium points $L_1$ and $L_2$ move further away from the rotating mass dipole, causing the Lyapunov orbit to become less deformed. Figure 20 shows the Lyapunov orbits for various mass ratios, considering the Jacobi constant $C^*$ = 3.01.

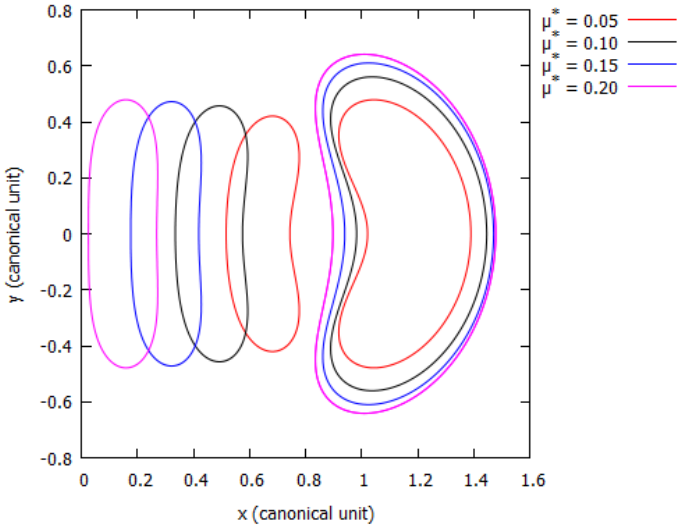


**Figure 20. Lyapunov orbits around the equilibrium points $L_1$ and $L_2$ for different mass ratios. $C^*$ = 3.01.**

## CONCLUSION

In this work, we performed an analysis of the Lyapunov planar orbits around the equilibrium points $L_1$ and $L_2$ in the restricted three-body synchronous problem. The initial estimates for orbits were found from the linearization of the equations of motion. In the modeling, we considered that one of the primary bodies was a mass point and the other one was modeled as a rotating mass dipole whose rotation is synchronous with the system. It is possible to notice that, when we take into account the elongated form of one of the primaries, compared to the restricted classical problem of three bodies, the trajectories found differ from each other, making the orbits in this model to suffer greater deviations due to the gravitational effects of $M_2$. It has been noted that the modification in the size of $M_2$ does not substantially alter the orbit's amplitude, but significantly affects the shape of the orbit, causing the Lyapunov orbit to become more deformed. We also made a numerical investigation modifying the mass ratio of the system. We found that, when we increase the mass ratio, the equilibrium point $L_1$ shifts considerably, making the Lyapunov orbit around this equilibrium point also to move away from $M_2$. On the other hand, the equilibrium point $L_2$ has a subtle displacement, as we increase the mass ratio of the system, making the Lyapunov orbits around $L_2$ to become egocentric.

The equilibrium points are considered as regions in space where they receive the least disturbance. So, these points are good places to hold a spaceship and can be used as parking orbits.

## Acknowledgements

The authors wish to express their appreciation for the support provided by grants# 406841/2016-0 and 301338/2016-7 from the National Council for Scientific and Technological Development (CNPq), and grants #2013/07174-4, #2014/22295-5, #2014/22295-5, # 2016/14665-2, 2016/18418-0, 2016/24561-0, 2018/00059-9 from São Paulo Research Foundation (FAPESP). We also are grateful for the financial support from the National Council for the Improvement of Higher Education (CAPES).

## REFERENCES

[1] E. Canalias and Josep J. Masdemont, "Homoclinic and heteroclinic transfer trajectories between planar Lyapunov orbits in the sun-earth and earth-moon systems." Discrete and Continuous Dynamical Systems. Vol. 14, No 2, 2016, pp. 261—279.

[2] 21st International Symposium on Space Flight Dynamics, ARTEMIS: "The First Mission to the Lunar Libration Orbits", September 28 - October 2 2009.

[3] M. Hechlera, M. Morab, M. Nogalesb, and A. Yezc, "Orbit Concepts at L2 for Soyuz Launches from Kourou," Acta Astronautica, Vol. 62, No. 2-3, 2008, pp. 140–150.

[4] Knutson, A. J., Howelly, Kathleen. "Using kane's method to incorporate attitude dynamics in the circular restricted three body problem" Advances in the Astronautical Sciences Vol. 143, pp. 2095

[5] Robert W. Farquhar, "The Flight of ISEE-3/ICE: Origins, Mission History, and a Legacy, "The Journal of the Astronautical Sciences, Vol. 49, No 1, 2001, pp. 23-73.

[6] D. Richardson, "Halo Orbit Formation for the ISEE-3 Mission," Journal of Guidance and Control, Vol. 3, No. 6, 1980, pp. 543–448.

[7] Huber, M., Bonnet, R., Dale, D., Arduini, M., Fröhlich, C., Domingo, V., and Whitcomb, G., "The History of the SOHO Mission," ESA Bulletin, Vol. 86, May 1996, pp. 25–35.

[8] A. Knutson and K. C. Howell, "Coupled orbit and attitude dynamics for spacecraft composed of multiple bodies in earth-moon halo orbits", 63rd International Astronautical Congress, paper IAC-12-C1.8.1.

[9] D. Folta, "Formation Flying Design and Applications in Weak Stability Boundary Regions," Annals of the New York Academy of Science, Vol. 1017, 2004, pp. 95–111.

[10] V.V. Radzievskii, "The restricted problem of three bodies taking account of light pressure." Astron. Zh. vol. 27, no. 5, pp. 250, 1950

[11] Y.A. Chernikov, "The photogravitational restricted problem of three bodies." Astron. Zh. vol. 47, pp. 217-223, 1970.

[12] K.B. Bhatnagar and J.M. Chawla, "A study of the Lagrangian points in the photogravitational restricted three-body problem" Indian J. Pure Appl. Math. vol. 10, no. 11, pp. 1443-1451, 1979.

[13] R.K. Sharma, "The linear stability of libration points of the photogravitational restricted three-body problem when the smaller primary is an oblate spheroid." Astrophys. Space Sci. vol. 135, no. 2, pp. 271-281, 1987.

[14] A.L. Kunitsyn and A.T. Tureshbaev, "On the collinear libration points in the photogravitational three-body problem." Celest. Mech. vol. 35 no. 2, pp. 105-112, 1985.

[15] L.G. Lukyanov, "On the family of the libration points in the restricted photogravitational three-body problem." Astron. Zh. vol. 65, pp. 422-432, 1988.

[16] Chermnykh, S.V.: Vestn. Leningr. Univ. **2**(8), 10 (1987).

[17] Kirpichnikov, S.N., Kokoriev, A.A.: Vestn. Leningr. Univ. **3**(1), 73 (1988).

[18] Kokoriev, A.A., Kirpichnikov, S.N.: Vestn. Leningr. Univ. **1**(1), 75 (1988).

[19] Zeng, X.Y., et al.: Astrophys. Space Sci. 356, 29 (2015).

[20] Ferrari, F., Lavagna, M., Howell, K.C.: Celest. Mech. Dyn. Astron. 125(4), 413 (2016).

[21] Zeng, X.Y., Fang, B.D., Li, J.F., et al.: Acta Mech. Sin. **32**(3), 535 (2016).

[22] Santos, L.B.T., Prado, A.F.B.A., Sanchez, D.M., "Equilibrium points in the restricted synchronous three-body problem using a mass dipole model"Astrophys. Space Sci. Vol. 362 No. 61, 2017, pp-60.

[23] Santos, L.B.T., Prado, A.F.B.A., Sanchez, D.M., "Equilibrium points around a double rotating mass dipole" COBEM. Procceedings of the 24th ABCM International Congress of Mechanical Engineering (2017).

[24] Santos, L.B.T., Prado, A.F.B.A., Sanchez, D.M.: Astrophysics and Space Science 362(11), 202 (2017).

[25] Wang Sang Koon, et al, "Heteroclinic Connections Between Periodic Orbits and Resonance Transitions in Celestial Mechanics," Chaos: An Interdisciplinary Journal of Nonlinear Science. Vol. 10, No 2, 2000.

[26] Szebehely, V. "Theory of Orbits". Academic Press, New York/London (1967).

[27] McCuskey, S.W. "Introduction to Celestial Mechanics", 1st edn. Addison-Wesley, Reading (1963).

[28] Dutt, P., Anilkumar, A.K.: Adv. Space Res. 54, 2050 (2014).

[29] Ren, Y., Shan, J.: Commun. Nonlinear Sci. Numer. Simul. 19, 554 (2014).

[30] Molton, F.R.: An Introduction to Celestial Mechanics, 4th edn. The Macmillan Company, New York (1960).

[31] Pushparaj, N., Sharma, R. K. "Halo Orbits at Sun-Mars L1, L2 in the Photogravitational Restricted Three-Body Problem with Oblateness" Advances in Astrophysics Vol. 2 No. 1, 2017, pp-35.

[32] J.D. Mireles James, "Celestial Mechanics Notes Set 4: The Circular Restricted Three Body Problem", 2006.

[33] J.D. Mireles James, "Celestial Mechanics Notes Set 5: Symmetric Periodic Orbits of the Circular Restricted Three Body Problem and their Stable and Unstable Manifolds", 2006.